22 December 2023

A Real-time Degradation Abatement Technique in Hybrid Electric Vehicle using Data-Driven Methods

Laxman Timilsina, Phuong H Hoang, Ali Moghassemi, Elutunji Buraimoh, Ali Arsalan, S M Imrat Rahman, Gokhan Ozkan, Behnaz Papari, Christopher S. Edrington

Abstract

The performance decline of Lithium-ion batteries due to degradation poses challenges for electric vehicles (EVs) and hybrid electric vehicles (HEVs) compared to traditional internal combustion engine vehicles. This research paper introduces a novel control architecture, named as Prognostic-Based Control Framework (PBCF), specifically designed for HEVs. The objective of PBCF is to minimize the overall operating costs of HEVs by considering the degradation of batteries used in the vehicle. The strategy leverages a degradation forecasting (DF) model for the battery to anticipate its degradation rate. The predicted degradation information is then utilized within the energy management (EM) system of the HEV to mitigate battery degradation. To predict the battery's capacity loss during vehicle operation, three different neural networks, namely the feedforward neural network (FNN), recurrent neural network (RNN), and deep neural network (DNN), are employed. The proposed strategy is implemented and validated under two different simulation environments. First in MATLAB/Simulink, and second, a real-time controller hardware-in-the-loop (CHIL) is set up. For the CHIL experiment, an HEV model is developed on Typhoon, a real-time simulator that communicates with other PBCF layers: the EM layer and the DF layer, which are deployed in Raspberry Pis, respectively. The communication between all these components occurs via the CAN protocol. The actual vehicle's operating conditions are transmitted from Typhoon to each Raspberry Pi and vice versa to facilitate the implementation of the proposed control strategy. The results from both numerical simulations and CHIL experiments demonstrate that this framework can effectively reduce the degradation of the battery and overall operating costs of the vehicle.

Keywords

Battery Life Prediction, Index Terms-Lithium-ion Battery, Re- maining Useful Life, battery degradation, hybrid electric vehicle, neural network, transportation

A Real-time Degradation Abatement Technique in Hybrid Electric Vehicle using Data-Driven Methods

Laxman Timilsina* Phuong H. Hoang◇ Ali Moghassemi* Elutunji Buraimoh* Ali Arsalan*
S M Imrat Rahman* Gokhan Ozkan† Behnaz Papari⅄ Christopher S. Edrington*

***Abstract*—The performance decline of Lithium-ion batteries due to degradation poses challenges for electric vehicles (EVs) and hybrid electric vehicles (HEVs) compared to traditional internal combustion engine vehicles. This research paper introduces a novel control architecture, named as Prognostic-Based Control Framework (PBCF), specifically designed for HEVs. The objective of PBCF is to minimize the overall operating costs of HEVs by considering the degradation of batteries used in the vehicle. The strategy leverages a degradation forecasting (DF) model for the battery to anticipate its degradation rate. The predicted degradation information is then utilized within the energy management (EM) system of the HEV to mitigate battery degradation. To predict the battery's capacity loss during vehicle operation, three different neural networks, namely the feedforward neural network (FNN), recurrent neural network (RNN), and deep neural network (DNN), are employed. The proposed strategy is implemented and validated under two different simulation environments. First in MATLAB/Simulink, and second, a real-time controller hardware-in-the-loop (CHIL) is set up. For the CHIL experiment, an HEV model is developed on Typhoon, a real-time simulator that communicates with other PBCF layers: the EM layer and the DF layer, which are deployed in Raspberry Pis, respectively. The communication between all these components occurs via the CAN protocol. The actual vehicle's operating conditions are transmitted from Typhoon to each Raspberry Pi and vice versa to facilitate the implementation of the proposed control strategy. The results from both numerical simulations and CHIL experiments demonstrate that this framework can effectively reduce the degradation of the battery and overall operating costs of the vehicle.**

***Index Terms*—Lithium-ion Battery, Battery Degradation, Remaining Useful Life, Battery Life Prediction, Hybrid Electric Vehicle, Neural Network**

I. Introduction

The growing apprehension surrounding greenhouse gas (GHG) emissions and their detrimental impact on the environment, coupled with the stringent emission regulations implemented by governments globally, has prompted the substitution of conventional internal combustion engine (ICE) vehicles with electrified vehicles. This transition towards electrified vehicles is also motivated by the imperative to address environmental pollution issues, volatility in petroleum product costs, and supply-demand challenges. Hybrid Electric Vehicles (HEVs) offer a promising solution because of their multiple power sources within the vehicle and their capability to harness energy during braking. Also, they possess an additional degree of freedom to meet the power requirements of the powertrain efficiently.

Despite electrified vehicles' advantages, their widespread adoption faces hurdles, notably high energy storage (ES) costs, limited charging infrastructure, and electrical source reliability [1]. ES expenses, particularly battery costs, represent a significant barrier, constituting around 30% of an electric vehicle's total cost [2]. The expenses associated with ES are considered a primary barrier, and reducing this cost is critical for enabling the swift expansion of electric transportation. To facilitate the rapid deployment of electric transportation, it is crucial to address and reduce the costs associated with the deterioration of ES systems [3].

In HEVs, the existence of multiple power generation sources necessitates the implementation of an energy management (EM) system [4]. The primary role of the EM system is to efficiently distribute power among the various power generation sources present within the vehicle with the objective of reducing fuel consumption [5], [6]. It is important to note that the control strategy employed by the EM system can significantly impact the degradation of the energy storage systems [5]. Numerous algorithms have been developed to optimize the performance of the EM system and minimize the degradation of the battery. Studies [7]–[9] have proposed the integration of supercapacitors (SCs) as hybrid energy storage systems alongside the battery. This configuration aims to reduce the stress on the battery during periods of high power demand, resulting in minimal degradation of the battery over time.

However, the inclusion of an additional device introduces additional costs to the vehicle. Furthermore, achieving effective minimization of battery degradation requires precise coordination among the engine, battery, and SC. This coordination adds complexity to the control algorithm of the EM system, surpassing the complexity of systems that solely utilize the battery as the ESS. Alternatively, in study [10], a cost-minimization model in the form of a predictive control problem is formulated to strike a balance between fuel consumption and battery degradation. This model takes into account factors

*L. Timilsina, E. Buraimoh, A. Arsalan, I. Rahman and C. S. Edrington are with the Real-Time COntrol and Optimization Laboratory (RT-COOL)-The Holcombe Department of Electrical and Computer Engineering-Clemson University, Clemson, SC 29634, USA. E-mails: $\{ltimils, amoghas, eburaim, aarsala, smimrar, cedring\}$@$clemson.edu$.

◇P. H. Hoang is a Power Systems Engineer in Operation Technology Inc, 17 Goodyear, Irvine, CA 92705. Email: $phuong.hoang$@$etap.com$.

†G. Ozkan, is with the Real-Time COntrol and Optimization Laboratory (RT-COOL)-The Holcombe Department of Electrical and Computer Engineering and a Research Assistant Professor at Dominion Energy Innovatin Center-Clemson University, North Charleston, SC. Email: $gokhano$@$clemson.edu$.

⅄B. Papari is with the Real-Time COntrol and Optimization Laboratory (RT-COOL)-The Holcombe Department of Electrical and Computer Engineering and an Assistant Professor at the Department of Automotive Engineering-Clemson University, Greenville, SC 29607. Email: $bpapari$@$clemson.edu$.

DISTRIBUTION STATEMENT A. Approved for public release: distribution is unlimited. (OPSEC 8117)

such as fuel consumption, electricity costs associated with battery charging/discharging, and the equivalent cost of battery degradation. However, it is important to note that this study does not consider all the major factors that contribute to the acceleration of battery degradation mechanisms. Moreover, the C/GMRES algorithm used in the study cannot handle the inequality constraints during optimization.

This study develops a constrained optimization algorithm for an EM system that can operate in real-time. The goal of the algorithm is to efficiently address the constraints of the EM strategy, specifically reducing fuel consumption costs. To achieve this, a set of constraints is established to govern the operation of the HEV within a specified range, emulating real-world driving conditions. The cost functions for minimizing battery aging are not included in the objective function of the EM, as this increases the complexity of the algorithm. Instead, a separate degradation forecasting (DF) layer is used to predict battery aging. This layer calculates the penalization cost as the battery degrades and communicates with the EM to update its objective function so as to minimize battery degradation.

A. Statement of Contributions

The contributions of this paper can be summarized as follows. Firstly, a prognostic-based control framework (PBCF) for HEVs is introduced, and its feasibility is validated under various operating conditions. The framework incorporates a battery degradation prediction model, employing different neural network (NN) models trained with battery cell data obtained from the University of Wisconsin-Madison. This degradation model is integrated into a new control layer, DF layer, above the existing EM layer in the HEV architecture. Thus, the proposed PBCF framework encompasses a multilayer control architecture consisting of the DF and EM layers, allowing for communication between them and the HEV model.

Secondly, the paper emphasizes real-time degradation abatement in HEVs. The predicted degradation rate obtained from the DF layer is used to calculate the penalized cost, which is then utilized to update the cost function of the EM system, aiming to minimize battery degradation while ensuring the vehicle functions optimally. Finally, the effectiveness of the proposed strategy is validated through numerical simulations and controller-hardware-in-the-loop (CHIL) experiments. These experiments demonstrate the cost-saving advantages of the proposed strategy and provide empirical evidence of its performance.

Furthermore, this study extends the previous research presented in the conference paper [11] by emphasizing the cost-saving advantages of the proposed strategy. To provide a comprehensive analysis, this study incorporates real-time CHIL experimentation in addition to conducting numerical simulations in MATLAB/Simulink. This expanded approach allows for a more thorough evaluation of the proposed strategy's effectiveness and its potential economic benefits by including two driving scenarios of the vehicle.

The remaining paper is structured as follows: Section II overviews the problem statement and the motivation driving the proposed strategy. In Section III, the vehicle architecture considered in this study is explained. Section IV presents all the techniques used to predict the degradation pattern of the battery, and Section V explains in detail the proposed control strategy, PBCF. The effectiveness of the proposed framework is evaluated through numerical simulations in Section VI. Section VII presents a CHIL experiment conducted to validate the proposed approach further. Finally, Section IX concludes the paper, summarizing the key findings and offering suggestions for future research directions.

II. Problem Formulation

Consider a series hybrid electric vehicle (HEV) that comprises two power generating sources, i.e., ICE and battery. The presence of multiple power-generating sources within the vehicle necessitates the implementation of an EM system. EM systems are commonly utilized in HEVs due to their fuel-saving capabilities [12]. However, it should be noted that different powertrain configurations may require distinct optimization formulations for the EM system, leading to varied strategies. In the case of a series HEV, as depicted in Fig. 1 (elaborated in Section III), the EM optimization for the reduction of fuel consumption can be generally formulated as follows:

$$\min \sum_{s \in \mathcal{S}} f_s\big(P_s(t_k)\big) \tag{1a}$$

$$P_s(t_k) \in \mathcal{P} \tag{1b}$$

where t_k is the time instant in the discrete domain, $\mathcal{S}$ is the set of indices of energy sources, and $P_s(t_k)$ is power generated by source s at t_k, and $\mathcal{P}$ is correspondingly the constraints set of $P_s(t_k)$, which are explained in detail in section V-2. For the sake of presentation, t_k is omitted.

The EM system's primary goal is to efficiently distribute power between the various sources to achieve economic objectives while considering system limitations [13]. Fuel consumption reduction is a key objective accomplished by allocating more power to the battery. However, it is essential to account for battery degradation as part of the operating cost. For instance, increased power allocation to the battery accelerates its degradation, leading to faster replacement and higher expenses for this costly component.

Therefore, the following two observations can be summarized from the EM's optimization problem:

- Observation 1: The EM system analyzes the operational state of the vehicle and determines the power references that need to be provided by the various power sources within the vehicle.
- Observation 2: The degradation process of the battery is influenced by the amount of power supplied by it or the operating condition of the battery itself. A higher power supply or power flow results in an increased degradation rate.

The battery's capacity gradually diminishes over time due to degradation, with varying degradation rates based on different operating conditions. Consequently, it becomes crucial to consider degradation costs when optimizing operating costs, taking into account the degradation pattern of the battery. To predict the degradation rate of the battery, a separate layer is defined as the DF layer. The EM system, in coordination with the proposed DF layer, can play a vital role in regulating the battery's degradation to meet the vehicle's load demands effectively.

Section V introduces a PBCF strategy, which involves predicting the degradation path of the battery. This predicted degradation path is then used to find a penalized cost that is integrated into the optimization problem of the EM system, allowing for the determination of optimal operation costs while considering degradation costs. Thus, this study presents an online data-driven approach for predicting the battery's degradation in a HEV. The predicted degradation is utilized to calculate the degradation cost, which subsequently modifies the objective function of the EM system (as represented by (1a)), with the objective of minimizing component degradation. Furthermore, the proposed strategy is verified under two driving conditions of the vehicle through MATLAB/Simulink and real-time CHIL simulations.

III. Hybrid Electric Vehicle Architecture

The HEV model employed in this study is extensively discussed in previous work [14], while the vehicle parameters and dynamics details are outlined in [15]. The vehicle parameters are obtained from the study [15] to calculate the reference power demanded by the powertrain for two specific drive cycles, namely US06 and WLTP. This series hybrid electric vehicle model incorporates a 600 V_{DC} bus, powered by an internal combustion engine (ICE) and a lithium-ion battery. Fig. 1 illustrates the powertrain architecture, where energy sources and loads are decoupled from the bus through the power electronics converters interface. Recent advancements in power electronics and cost reductions of power electronic devices have made this design economically viable [16], [17].

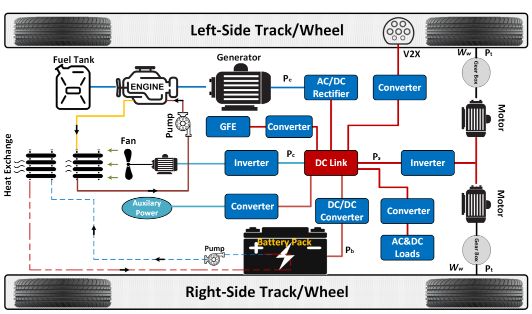

Fig. 1: Series HEV powertrain configuration considered in this paper.

The decoupling of energy sources and loads simplifies the implementation of the EM system by alleviating the complexities associated with power distribution in HEVs. Notably, this design relaxes various constraints related to propulsion load dynamics and the ICE. The series HEV model utilized in this project is constructed using the power flow equation of the vehicle. The model is implemented in MATLAB/Simulink for Section VI and in the digital real-time simulator Typhoon HIL 606 for Section VII.

IV. Degradation Modeling and Prediction

The degradation of any components occurs in all systems over time, with varying rates depending on their robustness and specific functions. In HEVs, different components experience a decrease in the life cycle count once they are in use. However, this particular study focuses on the deterioration of the power-generating sources used in HEVs. While internal combustion engines (ICE) can also degrade, batteries are especially susceptible to degradation [1]. This study focuses on battery degradation due to the prevalent use of HEVs with high hybridization factors (HF), which utilize batteries with larger capacities that can represent up to 30% of the total vehicle cost [11]. In automotive applications, the battery's lifespan is relatively shorter than other components, and it is considered unreliable once its capacity reaches 80% of the initial value [14]. Given the high initial cost of batteries, it is crucial to extend their lifespan for the economic viability of vehicle operation [18]. The longevity of a battery depends on its operation, and several factors, like temperature, charging and discharging currents, have different impacts on the degradation rate, which makes it a complex mechanism [19]–[21]. Battery degradation serves as a significant limiting factor in battery lifespan, necessitating thorough investigation and mitigation efforts to extend its longevity.

There are different types of modeling techniques for the degradation prediction of batteries. Study [14] employed an analytical approach, specifically utilizing a Markov chain model, to forecast battery degradation. However, this method possesses certain drawbacks. Firstly, when there is a large number of states, modeling with a Markov chain becomes intricate. Dealing with a substantial amount of data complicates the process. Also, predicting non-linear relationships using a Markov chain is challenging. Furthermore, an additional parameter, the transition matrix, needs to be calculated to develop the model. These limitations can be addressed by employing neural network models. In accordance with the insights provided by the study [22], various model-based, data-driven, and hybrid approaches have been utilized to predict the degradation trajectory. Several studies have used data-driven techniques, like studies [23], [24] have used convolutional neural networks to predict the degradation path of the battery. Consequently, considering that the previous study employed an analytical method, this current study adopts a data-driven approach utilizing diverse neural networks to model the battery's degradation trajectory.

To train the neural networks, enough historical aging data is needed, and recently, synthesized battery degradation datasets are also used as done in study [25]. However, this study utilizes a dataset from the University of Wisconsin-Madison, comprising multiple aging tests conducted at five distinct temperatures: $25°C$, $10°C$, $0°C$, $-10°C$, and $-20°C$ [26]. Each temperature setting includes ten unique aging datasets. Consequently, all these datasets were employed in the training, testing, and validation process of the neural networks. The patterns of aging data for each test are illustrated in Figure 2.

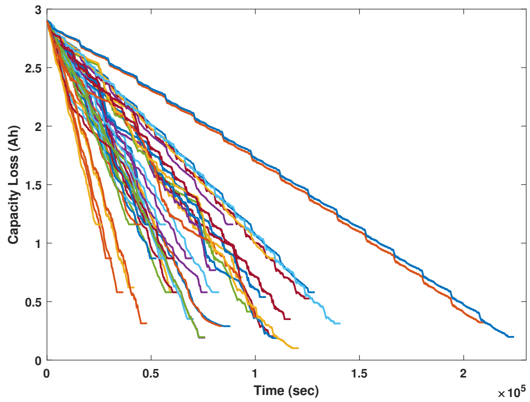

Fig. 2: Battery cell degradation dataset used to train the NNs.

A. Feed-Forward Neural Network based degradation model

In this section, a three-layer feedforward neural network architecture consisting of an input layer, a hidden layer, and an output layer is used to predict battery capacity loss. Before feeding the data to the model, they are pre-processed, and the necessary features are extracted: voltage, current, temperature, and capacity. The neural network's input layer accepts three inputs, namely current, voltage, and temperature, while the output layer predicts the capacity of the battery. The number of hidden layers is one, and the number of neurons is 32. The following sets of data denote the separation of data into training, testing, and validating data.

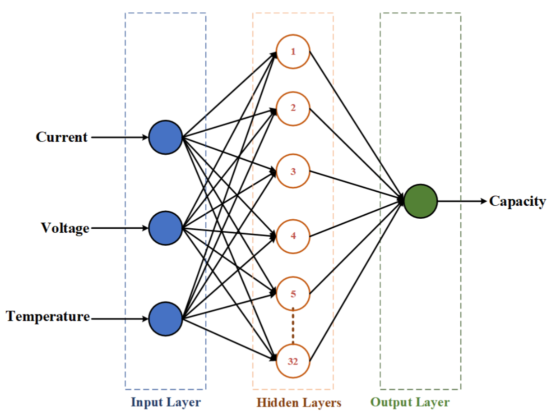

Fig. 3: A simple NN with three inputs and one output.

$$\delta_{train} = [(x_1, Y_1), (x_2, Y_2), (x_3, Y_3)..............(x_n, Y_n)] \quad (2)$$

$$\delta_{test} = [(x_{n+1}, Y_{n+1}), (x_{n+2}, Y_{n+2}), ...(x_s, Y_s)] \quad (3)$$

$$\delta_{validation} = [(x_{s+1}, Y_{s+1}), (x_{s+2}, Y_{s+2}), ...(x_t, Y_t)] \quad (4)$$

where x and Y represent the data extracted from the raw data. x is the input to the NN and has three variables voltage, current, and temperature as $x_i = (V_i, i_i, T_i)$. Similarly, Y is the output from the network, which represents the capacity of the battery. The δ_{train} is used to train the NN, whereas δ_{test} and $\delta_{validation}$ are used to test and validate the model developed using train data sets.

B. LSTM Neural Network based degradation model

A recurrent layer consists of specific neurons that have recurrent connections, allowing them to retain information from previous time steps, usually just one. This type of computational cell is highly advantageous when there is a need to capture the temporal dynamics of a sequence of inputs. In many cases, the output value is influenced by the historical context of the corresponding inputs. However, models like MLP or FNN as discussed earlier, are stateless, meaning their output is solely determined by the current input. To address this limitation, recurrent neural networks (RNNs) offer an internal memory mechanism that can capture both short-term and long-term dependencies, enabling them to retain and utilize information from previous time steps [27].

LSTM, which stands for Long Short-Term Memory, is a specific type of recurrent neural network (RNN) that addresses the challenges posed by the vanishing gradient problem and the need to capture long-term dependencies in sequential data [28]. LSTM has demonstrated its effectiveness in various applications, such as time series prediction, speech recognition, and natural language processing [29]. Given that battery degradation data is in the form of a time series, it is anticipated that employing an LSTM network for fitting or predicting battery aging would yield favorable outcomes. The detail of the RNN network is provided and compared with other networks in Table I.

C. Deep Neural Network (DNN) based degradation model

Deep neural networks (DNNs) are a type of artificial neural network that have multiple hidden layers between the input and output layers. The number of hidden layers is what makes a DNN "deep." The more hidden layers a DNN has, the more complex patterns and representations it can learn from data [30], [31]. DNNs have gained significant popularity in recent years and have been deployed successfully in various domains, including computer vision, natural language processing, speech recognition, and many other machine-learning tasks. The reasons why DNNs have been so successful are that they can learn complex patterns and representations from data, they can be trained on large amounts of data, and they are able to generalize to new data [32]. The detail of the DNN networks used in this study is provided and compared with other networks in Table I.

TABLE I: Structure of Different NNs

Parameters	**FNN**	**RNN (LSTM)**	**DNN**
Input Parameters	3	3	3
Hidden Layers	1	1	2
and Neurons	32	32 (LSTM cells)	32 and 16
Output Parameter	1	1	1
Optimizer	Adam	Adam	Adam
Loss Function	MSE	MSE	MSE

The construction and training of the above-mentioned three different neural network models are done using the PyTorch library in Python and deployed in Raspberry Pi 4 model B. The number of layers and neurons for these networks is summarized in Table I. As mentioned previously, the input data contains three features, namely voltage, current, and temperature. The number of hidden layers for all three networks is taken 32 (the first hidden layer of the DNN network) so as to compare the result from all these networks. The activation function applied in this layer is the Rectified Linear Unit (ReLU) function. ReLU is commonly used in hidden layers as it enables the model to learn intricate non-linear relationships, contributing to enhanced predictive performance [33]. Finally, the output layer consists of a single neuron to predict the capacity loss of the battery. No activation function is specified for the output layer, ensuring that it produces raw output values, directly representing the predicted continuous output.

The models are compiled using the mean squared error (MSE) as the loss function and the Adam optimizer. The MSE loss function measures the average squared difference between predicted and true output values. During training, the models use the Adam optimizer, which is a popular optimization algorithm known for its effectiveness in updating the model's parameters based on the calculated gradients.

The forward function is used for executing the forward pass of the model. It takes the input data, passes it through the hidden layer to obtain the hidden state, and then applies the fully connected layer to generate the output of the model. The models are trained and developed using the PyTorch library, which takes the training data and corresponding target values as defined in (2). The training is performed for 100 epochs, where the entire training dataset is passed through the network 100 times.

The diagram of the FNN is shown in Fig. 3 and for LSTM and DNN networks, the input and output parameters are the same; only the hidden layer and its neuron are different, which is provided in Table I. The main objective of the networks is to minimize the estimation error $J(\theta)$ and the difference between the actual capacity and the estimated capacity from the NN denoted by $f(x_i, \theta)$. To minimize this error, the Adam algorithm is used.

$$J(\theta) = \frac{1}{2}\sum_{i=1}^{n}(f(x_i,\theta) - Y_i)^2 \tag{5}$$

Fig. 4 depicts the forecasted degradation paths generated by these networks alongside the actual degradation path of the battery. Upon analyzing the figure, it becomes apparent that all three techniques exhibit good prediction performance. However, when comparing the three networks, the FNN exhibits the least accurate predictions. On the other hand, both the LSTM and DNN models demonstrate similar fitting capabilities. To assess the models more comprehensively, metrics such as mean absolute error (MAE), mean square error (MSE), and R-squared (R2) are used. The MAE provides an absolute measure of prediction accuracy, while the R2 value indicates how well the model captures the variability in the data.

Table II presents a comparison of the three techniques. The first three rows display the MAE, MSE, and R2 values for the testing dataset used during model training, while the last three rows exhibit the MAE, MSE, and R2 values for the unseen data that was not part of the training, testing, and validation process. It is evident from the table that the LSTM network outperforms the other two networks, exhibiting lower MAE values and higher R2 values for both the training/testing dataset and the unseen dataset. Additionally, the DNN model demonstrates the second-best fitting performance, while the FNN lags behind the other two models in terms of accuracy.

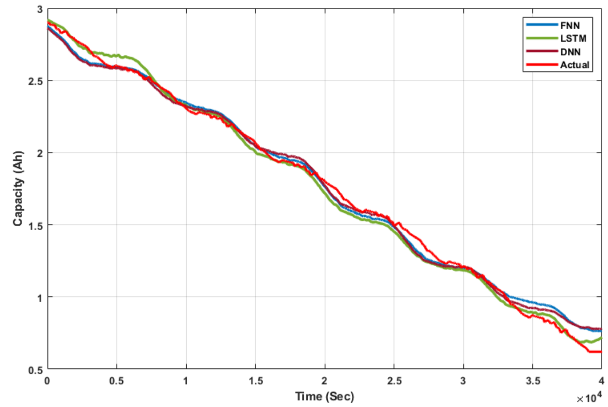

Fig. 4: Degradation prediction using different NNs.

TABLE II: Comparison of different NNs

Parameters	**FNN**	**LSTM**	**DNN**
MAE	0.0789	**0.0687**	0.0697
MSE	0.0129	**0.0091**	0.0096
R-square	0.9743	**0.984**	0.9808
MAE (new data)	0.8167	**0.0728**	0.0882
MSE (new data)	0.0212	**0.0088**	0.0119
R-square (new data)	0.9556	**0.9860**	0.9749

V. Prognostic Based Control Framework

This section introduces a framework for predicting and mitigating degradation. A multilevel control strategy (depicted in Fig. 5) is presented, comprising an upper layer just above an EM layer for degradation forecasting. The operations of each layer are comprehensively elucidated. This multilevel control strategy leverages advancements in computational technology, enabling cost-effective and streamlined vehicle operation.

Within this multilevel control architecture, the initial layer is the DF layer, which employs the NN degradation model to forecast the degradation of components. The subsequent layer is the EM layer, responsible for power allocation among sources in the vehicle. Lastly, the HEV model is deployed in the final layer. Section IV provides an explanation of the degradation modeling and prediction technique employed in this study. Section III previously discussed the configuration of the HEV model used in this study. Furthermore, the upcoming sections V-1 and V-2 detail the calculation of capacity loss of a battery using the proposed NNs and reconfiguring the EM optimization objective based on the DF layer's output.

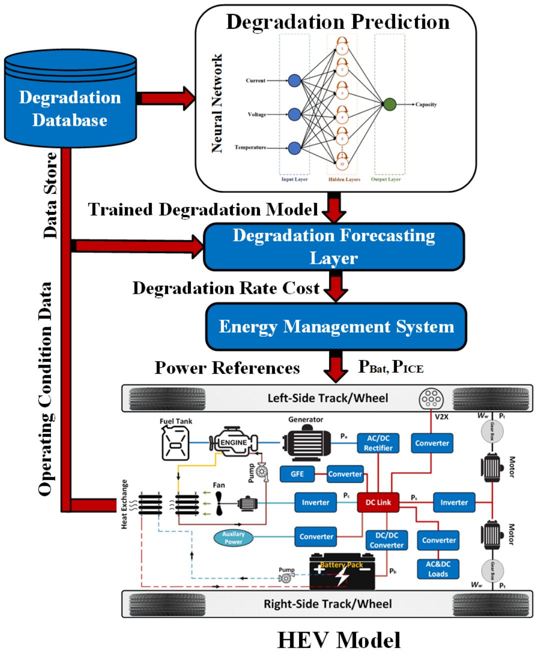

Fig. 5: Hierarchical control architecture.

1) Capacity Loss of Battery: In this section, a mechanism is presented to establish an interaction between the DF layer and the EM layer. This mechanism builds upon the degradation prediction methodology outlined in the preceding section. The approach involves incorporating a cost factor derived from the degradation results into the objective function of the EM layer. A few new parameters are introduced to quantify the degradation of component capacity. Let $\mathbb{P}_s(t_0)$ represent the maximum capacity of component s at the beginning when time is t_0, $\mathbb{P}_s(t_k)$ be the maximum anticipated capacity of the component s at time t_k. Also, let $\Delta_s(t_K)$ be the predicted capacity loss of the battery obtained from the degradation forecasting model using neural network, assuming the forecast of component degradation is conducted from t_0 to t_k. Then, the remaining capacity of the battery can be obtained using (6).

$$\mathbb{P}_s(t_K) = \mathbb{P}_s(t_0) - \Delta_s(t_K) \tag{6}$$

Assuming ρ_s represents the cost per unit of capacity of component s at the initial time, the degradation cost is accounted for by incorporating (7) into the objective cost of the EM layer. This is the parameter that is transferred from the DF layer to the EM layer.

$$f_s^d(P_s) = \rho_s \Delta_s P_s \tag{7}$$

2) Reconfiguration of EM's optimization problem: In Section II, EM was introduced and presented in a general mathematical form in (1a). This section comprehensively explains the EM's constraints and how the optimization problem is reconfigured. Traditionally, as discussed in Section II, the EM's optimization problem primarily focuses on reducing fuel costs. However, the degradation of electrical components, particularly batteries, presents a challenge and increases operating costs as they account for a significant portion of a vehicle's overall cost. Determining appropriate degradation cost is complicated since component degradation depends on their operating conditions. This task is performed by the DF layer in this study and sends the cost to the EM. Before that, the constraints for the EM are explained in detail. It is important to note that each energy source has its own generation capacity limits. In this study, two sources are considered, i.e., engine and battery; therefore, constraints in (1b) denote the lower and upper generation limits of each source.

$$\underline{P_{bat}} \leq P_{bat} \leq \overline{P_{bat}} \tag{8a}$$
$$\underline{P_{ICE}} \leq P_{ICE} \leq \overline{P_{ICE}} \tag{8b}$$

The primary objective of the powertrain is to ensure the proper supply of loads. The total generation should match the total load requirements, accounting for any losses. Given the specific configuration under consideration, constraint (9) is formulated.

$$P_{bat} + P_{ICE} = P_{AC\ load} + P_{DC\ load} + P_{propulsion} + P_{V2X} + P_{loss} \tag{9}$$

where P_{bat} and P_{ICE} are the power generated by the battery and engine, $P_{AC\ load}$ and $P_{DC\ load}$ are AC and DC loads, $P_{propulsion}$ is propulsion load, P_{V2X} is power used for V2X mode, and P_{loss} is the total loss encountered by the vehicle.

Each component utilized in a system has its own set of constraints. The power-generating sources employed in this study, namely ICE and battery, also have their internal constraints. Therefore, the following constraints are assumed for these power-generating sources.

$$|P_{ICE}(t_{k+1}) - P_{ICE}(t_k))| < rr_{ICE} \tag{10a}$$
$$|P_{bat}(t_{k+1}) - P_{bat}(t_k)| < rr_{bat} \tag{10b}$$
$$\underline{SoC_{bat}} \leq SoC_{bat} \leq \overline{SoC_{bat}} \tag{10c}$$
$$SOC_{bat}(t_{k+1}) = SOC_{bat}(t_k) - \frac{\delta T i_{bat}}{Q_{nom}} \tag{10d}$$

where $\delta T = t_{k+1} - t_k$. Constraints (10a) and (10b) are the ramp rate limits when adjusting their generation of power. Constraints (10c) and (10d) are the battery's State of Charge (SoC) constraint, where (10c) defines the operating range of SoC for battery and (10d) defines the equation for the change in battery's SoC during its operation.

The modification of the configuration of the EM's optimization problem allows for adjustments to the operating conditions of the components, i.e., sources in the vehicle. Two approaches can be employed to modify the operating conditions through EM: (a) changing the maximum generation capacities of the components and (b) modifying the EM's objective function. The operating conditions of the components are adjusted through the EM's objective function in this study, as changing the maximum capacity of sources in the HEV is not feasible. Recent research has placed emphasis on component degradation, and various studies have addressed this concern by incorporating degradation costs into the EM's objective function. For instance, in the study [34], a linear degradation cost is added to the EM's objective function. In [35], the degradation rate of a component is estimated from empirical data and used to construct an objective cost that considers degradation, investment, and fuel consumption costs. Similarly, in [36], the degradation cost is incorporated into the EM's objective function for different sources within a microgrid setup, aiming to minimize component degradation.

The proposed system is graphically represented in Fig. 5, where a NN degradation model is trained and utilized to predict the component's degradation, and subsequently, the degradation cost is calculated using (7) in the DF layer. The process of updating the objective function of the EM is like a feedback system, which is shown in Fig. 6. The EM's objective function is updated after incorporating the degradation cost, as shown in (11), through the proposed mechanism called the Prognostic-based control framework (PBCF).

$$\min \sum_{s\in\mathcal{S}} \big(f_s\big(P_s(t_k)\big) + f_s^d(P_s)\big) \tag{11}$$

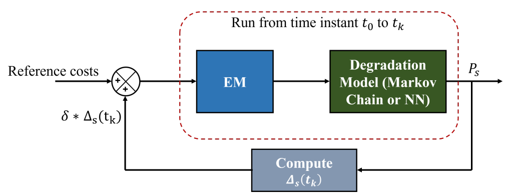

Fig. 6: Process involved while updating the objective function of EM.

Fig. 7 (b) depicts the optimized power distribution between the battery and ICE using the problem statement described in (1a). To address the degradation cost outlined in (7), it is incorporated into the EM's objective function. This inclusion results in the updated objective function presented in (11). Consequently, the power distribution between the ICE and battery is readjusted, as illustrated in Fig. 7 (c).

VI. Numerical Simulations

A. System description

In this section, numerical simulations are used to validate the proposed framework on a personal computer. The HEV powertrain, illustrated in Fig. 1 with two power sources, ICE and battery, is used for this purpose. Since this study focuses on reconfiguring the objective function of EM through the proposed framework, an HEV model based on the power flow equation is developed in MATLAB/Simulink. All vehicle parameters are considered from the study [15], which is then used to calculate the propulsion power for the US06 and WLTP drive cycles using Ansys Motor-CAD.

This study explores two distinct scenarios for validating the proposed control framework using different drive cycles. The first scenario employs the US06 drive cycle, encompassing a 598-second journey covering a distance of 8.01 miles in a single cycle, as shown in Fig. 7 (a). In contrast, the second scenario combines US06 and WLTP drive cycles, where one cycle lasts for 2398 seconds and runs for 22.46 miles, as shown in Fig. 7 (e). The reason behind this combination lies in the unique characteristics of the WLTP cycle, which includes frequent start-stop patterns, placing additional stress on the battery due to rapid accelerations during vehicle initiation. This amalgamation allows for assessing the proposed framework's effectiveness under varying levels of degradation induced by the vehicle's operational conditions.

Furthermore, it's important to highlight that the internal combustion engine (ICE) capacity within the HEV has the capacity to generate up to $180kW$, supplying power to the DC bus. Simultaneously, the HEV's battery possesses a capacity of $73kWh$. Of particular significance is the propulsion load, which consistently ranks as the most significant electrical load during vehicle operation. In this study, several cycles of propulsion load for each case are used. Additionally, the battery is operated within predefined SoC boundaries, with the lower limit set at 40% and the upper limit capped at 90%. To evaluate the economic feasibility of the proposed framework, it is essential to consider the initial cost of the battery. According to recent reports from [37], the average cost per kWh of a lithium-ion battery is around $\$151$ in 2023.

B. Numerical simulation results and discussion

The simulation is aimed to validate the proposed framework and perform a comparative analysis between two previously discussed scenarios. In each scenario, the simulation is conducted both with and without the application of PBCF. Moreover, where PCBF is employed, battery degradation predictions are made using an LSTM neural network, as described in Section IV. Additionally, this layer computes the degradation cost, a crucial factor integrated into the objective function of the EM system, as discussed in Section V.

1) Case-I: The US06 drive cycle, depicted in Fig. 7 (a), is employed in this case, consisting of a total duration of 598 seconds and covering a distance of 8.01 miles per cycle. The simulation is run for 75 consecutive drive cycles, equivalent to a total distance of 600 miles. The LSTM neural network degradation model developed in Section IV is utilized to predict the degradation path of the battery. The power allocation by the EM before and after implementing the PBCF is illustrated in Fig. 7 (b) and (c). The implementation of PBCF results in a notable change in the power allocation to the battery and the engine. This is evident from these two graphs, where the ICE also supplies additional power compared to the previous case (i.e., without PBCF) to meet the vehicle's load demand. The developed framework is designed to navigate the trade-off between fuel cost and battery degradation. It aims to determine an optimal point at each instance where both the battery and engine supply power to meet the power demand, with the goal of minimizing the overall operating cost by reducing the degradation of the battery. Fig. 7 (d) showcases a reduction in the degradation path after implementing PBCF. The capacity loss of the battery without PBCF is found to be 0.1848%, whereas the capacity loss with PBCF is observed to be 0.1561% after driving for 75 drive cycles. Fig. 7 (e) provides valuable insights into the economic implications of implementing the PBCF strategy. The results show a saving in the degradation costs of the battery, amounting to $15.82. However, it is important to note that there is an increase in fuel cost of $6.7019 due to the higher power supplied by the ICE. Nevertheless, when considering the overall operating costs, the PBCF strategy resulted in a net reduction of $9.1181 after 75 drive cycles.

2) Case-II: To evaluate the feasibility and effectiveness of the proposed strategy across various driving scenarios, a drive cycle is created by combining the characteristics of two distinct drive cycles: the US06 and WLTP drive cycles. The inclusion of the WLTP drive cycle is driven by its ability to replicate real-world driving conditions, incorporating a range of driving maneuvers such as starts, accelerations, and stops within a controlled environment, which is shown in Fig. 7 (f). In the combined drive cycle, the vehicle initially runs with the US06 drive cycle for a duration of 598 seconds. Following this period, the WLTP drive cycle is seamlessly integrated, extending for a duration of 1800 seconds. Throughout this combined drive cycle, the vehicle covers a total distance of 22.46 miles. The vehicle operates under the US06 drive cycle for 8.01 miles, replicating the corresponding driving conditions and load profiles associated with this specific drive cycle. Subsequently, the vehicle transitions to the WLTP drive cycle, covering an additional distance of 14.45 miles. The propulsion load profile, as illustrated in Fig. 7 (f), provides valuable insights into the power demands and fluctuations experienced by the vehicle throughout the combined drive cycle.

The power allocation by the EM system before and after implementing PBCF is depicted in Fig. 7 (g) and (h), respectively. Initially, during the US06 drive cycle, the power distribution is similar as discussed in the previous section. However, as the drive cycle transitions to the WLTP phase beyond 598 seconds, a different power allocation pattern emerges. During this phase, the power demand from the vehicle decreases, and the battery becomes capable of meeting the vehicle's power requirements independently until 2100 seconds. The ICE remains inactive until the power demand exceeds the battery's capacity, at which point it engages to fulfill the additional power needs.

Lastly, Fig. 7 (i) showcases a reduction in the degradation path after implementing PBCF. The reason for the minimization of the degradation is ICE also supplies the power during acceleration of the vehicle, as shown in Fig. 7 (h), so that there is less stress on the battery. The capacity loss of the battery without PBCF is found to be 0.2679%, whereas the capacity loss with PBCF is observed to be 0.2325% after driving for 27 drive cycles. Fig. 7 (j) provides valuable insights into the economic implications of implementing the PBCF strategy. The results show a reduction in the degradation costs of the battery, amounting to $19.47. However, it is important to note that there is an increase in fuel cost of $8.49 due to the higher power supplied by the ICE. Nevertheless, when considering the overall operating costs, the PBCF strategy resulted in a net reduction of $10.98 after 27 drive cycles.

The results obtained from this numerical simulation are cross-referenced with the outcomes of the CHIL experiment, as well as the findings from the study [14]. This comparative analysis is detailed in Section VII, Tables III and IV, respectively.

VII. CHIL Experiment

The controller hardware-in-the-loop (CHIL) experiments are conducted to test and validate algorithms or frameworks in real-time systems using real-time simulators and controllers [38]. Therefore, the execution of the proposed strategy is exemplified through a CHIL experiment. To facilitate this, state-of-the-art equipment from Clemson University's Real-time Control and Optimization Laboratory (RT-COOL) is harnessed, effectively integrating the DF layer with the EM layer. Subsequent sections will provide in-depth insights into the CHIL implementation process and the ensuing experimental findings.

A. System modeling

The series HEV developed as explained in Section III is deployed in Typhoon HIL using a schematic editor in its control center software. This model is then compiled and integrated into the HIL SCADA system before being deployed into the digital real-time simulator Typhoon HIL 606.

To effectively manage multiple power sources within a vehicle, the use of an EM system becomes imperative, as explained in Section II. The EM algorithms are typically implemented within a control unit referred to as an electronic control unit (ECU) in the vehicles. In this context, a Raspberry Pi 4 model B is used as an ECU to execute the EM algorithm. The primary objective of this algorithm, as elaborated upon in detail in Section II, is to minimize fuel costs. Real-time operational data from the HEV model (Typhoon) is transmitted to the Raspberry Pi, where the EM algorithm is executed to determine the optimal reference power levels to be provided by both the battery and the ICE. Subsequently, these reference power values are relayed back to the Typhoon system. In automotive applications, the prevalent communication protocol employed is Controller Area Network (CAN) communication. Therefore, for this study, CAN communication is utilized to facilitate data exchange between the simulator and the ECUs.

B. Integrating degradation forecasting into the EM

In the preceding Section VII-A, the real-time implementation of the EM system in conjunction with the developed HEV model was explained. In the proposed strategy (PBCF), an additional layer known as the DF layer is seamlessly integrated above the EM. For this, another Raspberry Pi, designated as ECU-2, is used where the neural network model developed in Section IV is deployed. The neural network model is trained on the Pi itself, and with the help of a PC acting as a server, this model is obtained on this specific Pi. The server's functionalities involve sending trained models whenever the real-time controller that implements the DF requests them and stores the necessary scripts for the EM and DF in their respective controllers. Finally, with the help of a trained neural network, the DF layer predicts the degradation of the battery and calculates the degradation rate cost using (7). Subsequently, this computed cost is transferred to the Energy EM system. The EM, in turn, integrates this cost as a penalty factor within its objective function. This adjustment prompts the EM to optimize power allocation among the two sources present in

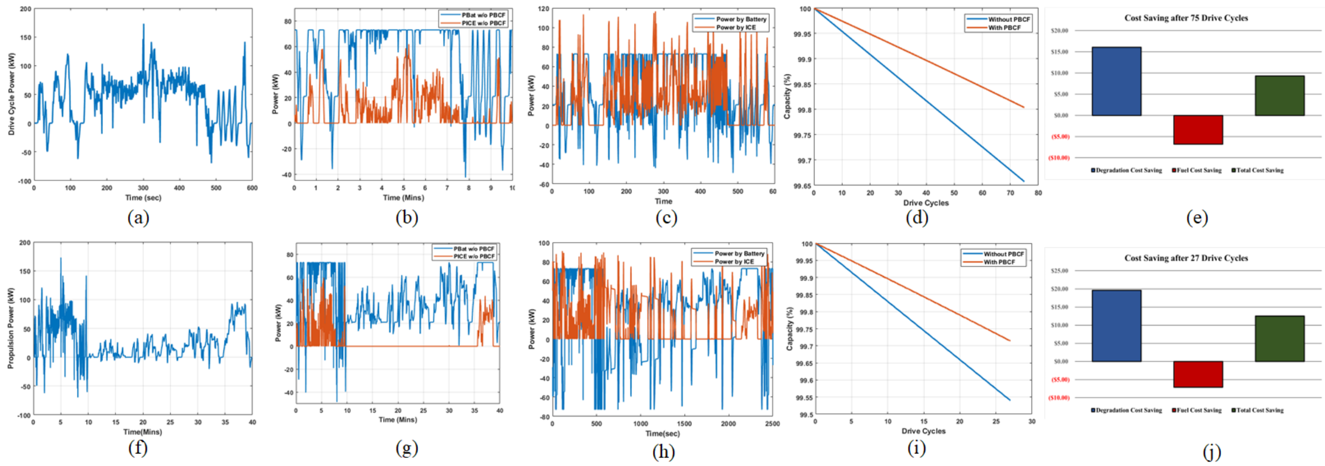

Fig. 7: Case-I simulation results: (a) A sample of propulsion load for US06 drive cycle (b) Power allocated by EM without PBCF (c) Power allocated by EM with PBCF (d) Battery degradation abatement using PBCF (e) Cost saving using PBCF. Case-II simulation results: (f) A sample of propulsion load for US06 drive cycle (g) Power allocated by EM without PBCF (h) Power allocated by EM with PBCF (i) Battery degradation abatement using PBCF (i) Cost saving using PBCF..

the vehicle. The effective communication between the ECUs and the digital real-time simulator is seamlessly facilitated through CAN communication, as elaborated in the following section.

C. Communication

The Controller Area Network (CAN) is a widely adopted communication protocol for data transmission within automotive applications. Within a CAN network, data exchange occurs between various ECUs, also referred to as nodes. This communication takes place through a pair of wires known as CAN HIGH (CAN-H) and CAN LOW (CAN-L). All nodes are interconnected via the CAN bus. When a node intends to transmit data, it first checks the bus to ascertain its availability. If the bus is unoccupied, the node proceeds to transmit its message by placing it onto the bus. Each node within the network receives this message and scrutinizes its identifier. Each message comprises an identifier, which delineates the message's priority and content alongside the data to be conveyed.

Within the scope of this study, three distinct nodes are present, as delineated below:

- Typhoon (HEV Model)
- Raspberry Pi (ECU-1, EM)
- Raspberry Pi (ECU-2, DF)

Data transmission within a CAN network involves transmitting data from a single node onto the CAN bus, which can be accessed by all other nodes connected to the network. In this study, the establishment of a CAN network is facilitated by Typhoon, which employs its own interface incorporating CAN send and CAN receive blocks to enable data transmission. To facilitate targeted communication, specific message IDs are assigned for the transmission of data to particular ECUs. On the receiving side, these message IDs are validated to ensure that the intended ECU correctly receives the data. Similarly, for Raspberry Pis, Python code is scripted to facilitate data exchange over the CAN bus. This methodology empowers each of the aforementioned nodes to transmit and receive signals utilizing distinct message IDs, thereby ensuring dependable communication while minimizing interference. The depiction of CAN communication integration within RT-COOL is shown in Fig. 8.

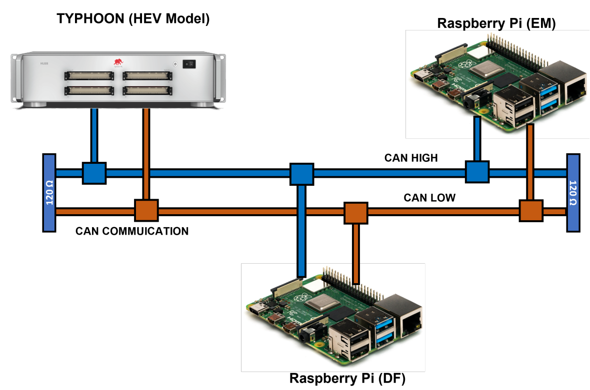

Fig. 8: CHIL implementation of PBCF in real-time on actual components in RT-COOL.

D. Visualization

Human-Machine Interface (HMI) is designed for system monitoring using a HIL SCADA window within the Typhoon control center, complemented by a Python visualization environment. The Typhoon system collects operational data from various sources, including the simulator and all ECUs, and displays this data within the SCADA window.

The HMI encompasses four key screens: the control screen, HEV monitoring screen, energy management screen, and degradation forecasting screen. The control screen incorporates start/stop buttons and input fields for CHIL system details, including IP addresses for all controllers (ECUs), simulators, and the host PC. The HEV monitoring screen provides insights

Fig. 9: (a) Visualization screen for CHIL experiment in SCADA window in Typhoon control center (b) Control screen for CHIL implementation (c) HMI display for HEV model parameters in real-time (d) HMI display for EM layer parameters in real-time (e) HMI display for DF layer parameters in real-time.

into the loads requested by the series HEV, the vehicle's speed, and the SoC of the vehicle's battery. Users have real-time control over most loads while the system is operational, with the exception of the propulsion load, given that the vehicle adheres to a predefined drive cycle.

The energy management screen displays data transmitted by the EM controller to the Typhoon, revealing how the EM allocates power to the battery and ICE to meet the vehicle's power demands with and without PBCF. Lastly, the degradation forecasting screen illustrates the battery's degradation trajectory and its remaining capacity, received from the DF controller, along with degradation rate cost, fuel cost, and the total savings obtained through the proposed control strategy.

Fig. 9 (b) provides an overview of the primary control implementation screen. Upon pressing the start button, the CHIL experiment commences. Before initiating the experiment, the user must select the Python executable file, as all the project's code is written in Python. Additionally, the directory containing all the necessary project code must be specified within the CHIL folder, as depicted in the figure. Fig. 9 (a) showcases the primary monitoring screen, comprising three subsections: HEV monitoring, EM layer, and DF Layer. Each subsection presents results from different controllers. Fig. 9 (d) offers insight into the parameters of the HEV considered in this project, while Fig. 9 (c) showcases the optimized results transmitted from the EM layer to the Typhoon. Fig. 9 (e) presents results from the DF layer.

E. Experimental results

Fig. 10 offers a visual representation of the results stemming from the CHIL experiment, distinctively highlighting the outcomes for both Case I and Case II, as explained in Section VI. Detailed explanations for the results of each of these cases are provided in the following sections.

1) Case-I: As mentioned earlier, the US06 drive cycle is used for the simulation. The CHIL simulation is run for 75 consecutive drive cycles, equivalent to a total distance of 600 miles. The power allocation by the EM before the implementation of the PBCF is the same as shown in Fig. 7 (b). However, after implementing PBCF, the allocation of power among the energy sources takes a distinct shape, as depicted in Fig. 10 (a). This variation in the power allocation graph is attributed to the utilization of the LSTM NN within the CHIL experiment.

From both simulations, it's evident that the introduction of PBCF brings about a significant shift in the power distribution between the battery and the internal combustion engine (ICE). The ICE also contributes additional power to fulfill the vehicle's load requirements. Fig. 10 (b) showcases a reduction in the degradation trajectory following PBCF implementation. The capacity loss of the battery without PBCF amounts to 0.1848%, whereas, with PBCF in place, it reduces to 0.1561% after 75 drive cycles.

Fig. 10 (c) and Fig. 10 (d) delve into the economic implications of PBCF adoption. Fig. 10 (c) illustrates savings achieved with PBCF concerning cycle numbers, while Fig. 10 (e) provides a bar chart of savings after 75 drive cycles. These results demonstrate a cost reduction in battery degradation expenses, tallying up to \$15.82. Nevertheless, it's noteworthy that there's an increase in fuel costs, amounting to \$6.7019, attributed to the higher power supplied by the ICE. However, when considering the overall operational costs, the implementation of the PBCF strategy yields a net reduction of \$9.1181 after 75 drive cycles.

2) Case-II: A combined drive cycle using US06 and WLTP is used for the simulation in this case. The CHIL simulation is run for 27 consecutive drive cycles, equivalent to a total distance of 606 miles. The power allocation by the EM before the implementation of the PBCF is the same as shown in Fig. 7 (g). However, after implementing PBCF, the allocation of power among the energy sources takes a distinct shape, as depicted in Fig. 10 (e) as discussed in the previous case.

From both simulations, it's evident that the introduction of PBCF brings about a significant shift in the power distribution between the battery and the ICE. The ICE also contributes additional power to fulfill the vehicle's load requirements. Fig. 10 (f) showcases a reduction in the degradation trajectory following PBCF implementation. The capacity loss of the battery without PBCF amounts to 0.1848%, whereas, with PBCF, it reduces to 0.1561% after 75 drive cycles.

Fig. 10 (g) and (h) delve into the economic implications of PBCF adoption. Fig. 10 (g) illustrates savings achieved with PBCF concerning cycle numbers, while Fig. 10 (h) provides a bar chart of savings after 75 drive cycles. These results demonstrate a cost reduction in battery degradation expenses, tallying up to \$19.63. Nevertheless, it's noteworthy that there's an increase in fuel costs, amounting to \$7.11, attributed to the higher power supplied by the ICE. However, when considering the overall operational costs, the implementation of the PBCF strategy yields a net reduction of \$12.52 after 27 drive cycles.

VIII. Comparison between Numerical Simulation and CHIL Experiment Results

The presented framework is simulated using MATLAB and real-time CHIL experiments to verify its validity. This section conducts a comparative analysis of the results derived from these distinct simulation environments. Table III offers an assessment of capacity loss observed in these simulations. In Case I, the capacity loss in battery between NS and CHIL simulations exhibits disparities, while the capacity loss saving post-PBCF implementation demonstrates substantial similarity, with the capacity savings amounting to 0.1464% in NS and 0.146% in CHIL. Similarly, in Case II, the capacity loss remains nearly identical with and without PBCF implementation. Regarding NS, the capacity loss saving equals 0.1732% in NS and 0.1787% in the CHIL experiment.

TABLE III: Comparison of different parameters for NS and CHIL experiment.

Method	NN (Case-I)	NN (Case-II)
Capacity Loss without PBCF (NS)	0.3425%	0.4588%
Capacity Loss with PBCF (NS)	0.1961%	0.2856%
Capacity Loss without PBCF (CHIL)	0.4397%	0.4523%
Capacity Loss with PBCF (CHIL)	0.2937%	0.2736%

Again, Table IV facilitates a comparison of savings following the implementation of PBCF across three scenarios. The findings from [14] are incorporated to compare with the outcomes presented in this paper. It is noteworthy to highlight that in [14], simulations were conducted at $25°C$ to have normal battery degradation during vehicle operation. In contrast, this study conducts simulations at $10°C$ to intentionally induce a higher degree of degradation compared to [14]. This approach aims to assess the performance of PBCF under varying levels of degradation.

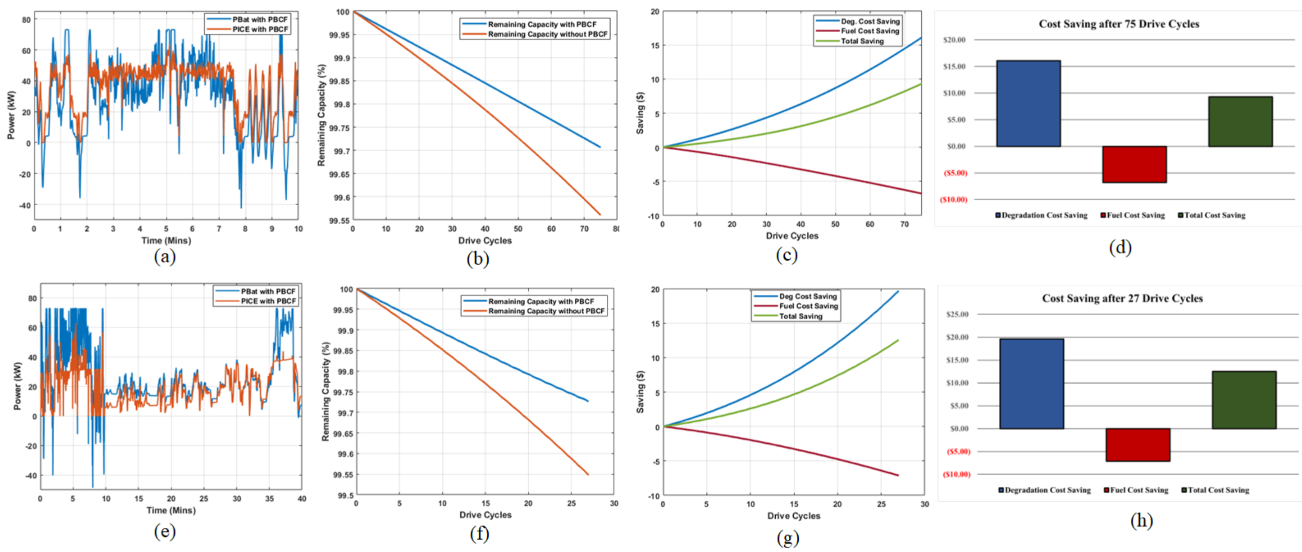

Fig. 10: Case-I simulation results: (a) Power allocated by EM with PBCF (b) Battery degradation abatement using PBCF (c) Cost saving using PBCF over different cycles (d) Cost saving using PBCF after 75 drive cycles.
Case-II simulation results: (e) Power allocated by EM with PBCF (f) Battery degradation abatement using PBCF (g) Cost saving using PBCF over different cycles (h) Cost saving using PBCF after 27 drive cycles.

The table encompasses all cost analyses considered within this project, including degradation cost, fuel cost, and total savings, which represent the difference between the first two costs. Examination of the table reveals that in the neural network simulation, both cases yield nearly identical values for various cost factors and the resultant total savings. However, slight discrepancies emerge between the NS and CHIL experiment results from [2], which employ a Markov Chain Model. Nevertheless, PBCF's primary contribution remains consistent across all three scenarios, regardless of whether the simulation is conducted in MATLAB or via CHIL experiments. It consistently reduces battery degradation and lowers the overall operating cost of the vehicle.

Moreover, it's noteworthy that as battery degradation increases, the savings after PBCF implementation also rise, as evidenced by the outcomes in these three scenarios.

TABLE IV: Comparison of savings after implementing PBCF

Method	**Markov Chain [14]**	**NN Case-I**	**NN Case-II**
Degradation Cost (NS)	$10.80	$15.82	$19.47
Degradation Cost (CHIL)	$8.26	$16.09	$19.63
Fuel Cost (NS)	-$5.98	-$6.70	-$8.49
Fuel Cost (CHIL)	-$4.92	-$6.78	-$7.11
Total Saving (NS)	$4.8	$9.11	$10.98
Total Saving (CHIL)	$3.33	$9.31	$12.52

IX. Conclusion and Future Work

This paper introduces a Prognostic-Based Control Framework (PBCF) that integrates a degradation forecasting layer into the existing control architecture of an HEV. The objective is to minimize battery degradation and consequently reduce overall operational costs. Three distinct neural network-based degradation models were constructed to predict the degradation patterns of the battery used in HEVs. These models were trained using battery data from the University of Wisconsin-Madison. Among the FNN, LSTM, and DNN, the LSTM neural network demonstrated superior fitting, leading to its selection for battery degradation prediction.

The predictions generated by the LSTM neural network were employed to compute degradation costs, which were subsequently integrated into the objective function of the EM system. The effectiveness of this approach was validated through numerical simulations conducted in MATLAB/Simulink and CHIL experiments utilizing laboratory equipment. Both simulation methods indicated cost savings in the operation of the studied system and a reduction in battery degradation. Additionally, the outcomes from this study were compared to those derived from the Markov Chain model, and they produced consistent results.

Furthermore, the proposed framework was subjected to testing at varying levels of battery degradation, and it was observed that higher levels of battery degradation corresponded to greater savings after implementing PBCF.

Acknowledgments

This work was supported by Clemson University's Virtual Prototyping of Autonomy Enabled Ground Systems (VIPR-GS), under Cooperative Agreement W56HZV-21-2-0001 with the US Army DEVCOM Ground Vehicle Systems Center (GVSC).

DISTRIBUTION STATEMENT A. Approved for public release: distribution is unlimited. (OPSEC 8117)

References

[1] P. Hoang and et. al., "A Prognostic Based Control Framework For Hybrid Electric Vehicles," *SAE Technical Paper*, pp. 1–8, 2022.

[2] Bloomberg, "Batteries for electric cars speed toward a tipping point," vol. 134, 2020. [Online]. Available: http://bloomberg.com

[3] S. Paudel, J. Zhang, B. Ayalew, M. Castanier, and A. Skowronska, "A model predictive control-based operation of vehicle-borne microgrid considering battery degradation," in *Proceedings of the Ground Vehicle Systems Engineering and Technology Symposium*, pp. 15–17.

[4] S. Onori, L. Serrao, and G. Rizzoni, "Hybrid electric vehicles: Energy management strategies," 2016.

[5] L. Serrao, S. Onori, and G. Rizzoni, "A comparative analysis of energy management strategies for hybrid electric vehicles," 2011.

[6] X. Lü, Y. Wu, J. Lian, Y. Zhang, C. Chen, P. Wang, and L. Meng, "Energy management of hybrid electric vehicles: A review of energy optimization of fuel cell hybrid power system based on genetic algorithm," *Energy Conversion and Management*, vol. 205, p. 112474, 2020.

[7] J. Du, X. Zhang, T. Wang, Z. Song, X. Yang, H. Wang, M. Ouyang, and X. Wu, "Battery degradation minimization oriented energy management strategy for plug-in hybrid electric bus with multi-energy storage system," *Energy*, vol. 165, pp. 153–163, 2018.

[8] T. Zhu, R. Lot, R. G. Wills, and X. Yan, "Sizing a battery-supercapacitor energy storage system with battery degradation consideration for high-performance electric vehicles," *Energy*, vol. 208, p. 118336, 2020.

[9] L. Kouchachvili, W. Yaïci, and E. Entchev, "Hybrid battery/supercapacitor energy storage system for the electric vehicles," *Journal of Power Sources*, vol. 374, pp. 237–248, 2018.

[10] N. Guo, X. Zhang, Y. Zou, L. Guo, and G. Du, "Real-time predictive energy management of plug-in hybrid electric vehicles for coordination of fuel economy and battery degradation," *Energy*, vol. 214, p. 119070, 2021.

[11] L. Timilsina, P. H. Hoang, A. Arsalan, G. Ozkan, B. Papari, and C. S. Edrington, "Degradation abatement in hybrid electric vehicles using data-driven technique," *Transportation Research Procedia*, 2023.

[12] D. Bianchi, L. Rolando, L. Serrao, S. Onori, G. Rizzoni, N. Al-Khayat, T.-M. Hsieh, and P. Kang, "A rule-based strategy for a series/parallel hybrid electric vehicle: an approach based on dynamic programming," in *Dynamic Systems and Control Conference*, vol. 44175, 2010, pp. 507–514.

[13] Z. Song, H. Hofmann, J. Li, J. Hou, X. Han, and M. Ouyang, "Energy management strategies comparison for electric vehicles with hybrid energy storage system," *Applied Energy*, vol. 134, pp. 321–331, 2014. [Online]. Available: http://dx.doi.org/10.1016/j.apenergy.2014.08.035

[14] L. Timilsina, P. H. Hoang, G. Ozkan, B. Papari, and C. S. Edrington, "A real-time prognostic-based control framework for series hybrid electric vehicles," *IEEE Access*, 2023.

[15] Q. Zhu, A. Kumar, A. Sundar, D. Egan, H. Mirzaei, D. Chang, M. Schmid, R. Prucka, B. Lawler, and C. Paredis, "Development of a series hybrid electrified powertrain for a high speed tracked vehicle based on driving cycle simulation," *SAE International Journal of Advances and Current Practices in Mobility*, vol. 4, no. 2022-01-0367, pp. 1403–1412, 2022.

[16] P. K. Chamarthi, C. Edrington, A. Arsalan, L. Timilsina, B. Papari, G. Ozkan, and A. Moghassemi, "A novel 1-ϕ cuk based on-board electric vehicle charger with minimal number of power components," SAE Technical Paper, Tech. Rep., 2023.

[17] S. M. I. RAHMAN, A. Moghassemi, A. Arsalan, L. Timilsina, P. K. Chamarthi, B. Papari, G. Ozkan, and C. S. Edrington, "Emerging trends and challenges in thermal management of power electronic converters: A state of the art review," *IEEE Access*, 2023.

[18] N. Sapkota, S. Chiluwal, P. Parajuli, A. Rowland, and R. Podila, "Insights into the pseudocapacitive behavior of sulfurized polymer electrodes for li–s batteries," *Advanced Science*, p. 2206901, 2023.

[19] Z. M. Ali, M. Calasan, F. H. Gandoman, F. Jurado, and S. H. A. Aleem, "Review of batteries reliability in electric vehicle and e-mobility applications," *Ain Shams Engineering Journal*, p. 102442, 2023.

[20] A. Tomaszewska, Z. Chu, X. Feng, S. O'kane, X. Liu, J. Chen, C. Ji, E. Endler, R. Li, L. Liu *et al.*, "Lithium-ion battery fast charging: A review," *ETransportation*, vol. 1, p. 100011, 2019.

[21] S. M. Sabet, N. Sapkota, S. Chiluwal, T. Zheng, C. M. Clemons, A. M. Rao, and S. Pilla, "Sulfurized polyacrylonitrile impregnated delignified wood-based 3d carbon framework for high-performance lithium–sulfur batteries," *ACS Sustainable Chemistry & Engineering*, vol. 11, no. 6, pp. 2314–2323, 2023.

[22] L. Timilsina, P. R. Badr, P. H. Hoang, G. Ozkan, B. Papari, and C. S. Edrington, "Battery degradation in electric and hybrid electric vehicles: A survey study," *IEEE Access*, 2023.

[23] N. Costa, L. Sanchez, D. Ansean, and M. Dubarry, "Li-ion battery degradation modes diagnosis via convolutional neural networks," *Journal of Energy Storage*, vol. 55, p. 105558, 2022.

[24] S. Kim, H. Jung, M. Lee, Y. Y. Choi, and J.-I. Choi, "Model-free reconstruction of capacity degradation trajectory of lithium-ion batteries using early cycle data," *eTransportation*, vol. 17, p. 100243, 2023.

[25] M. Dubarry, C. Truchot, and B. Y. Liaw, "Synthesize battery degradation modes via a diagnostic and prognostic model," *Journal of power sources*, vol. 219, pp. 204–216, 2012.

[26] K. P., "Panasonic 18650pf li-ion battery data," https://data.mendeley.com/datasets/cp3473x7xv/3, note = Accessed: 06/11/2022.

[27] A. Arsalan, L. Timilsina, B. Papari, G. Muriithi, G. Ozkan, P. Kumar, and C. S. Edrington, "Cyber attack detection and classification for integrated on board electric vehicle chargers subject to stochastic charging coordination," *Transportation Research Procedia*, 2023.

[28] Y. Zhang, R. Xiong, H. He, and M. G. Pecht, "Long short-term memory recurrent neural network for remaining useful life prediction of lithium-ion batteries," *IEEE Transactions on Vehicular Technology*, vol. 67, no. 7, pp. 5695–5705, 2018.

[29] J. Lu, R. Xiong, J. Tian, C. Wang, C.-W. Hsu, N.-T. Tsou, F. Sun, and J. Li, "Battery degradation prediction against uncertain future conditions with recurrent neural network enabled deep learning," *Energy Storage Materials*, vol. 50, pp. 139–151, 2022.

[30] B. Zraibi, C. Okar, H. Chaoui, and M. Mansouri, "Remaining useful life assessment for lithium-ion batteries using cnn-lstm-dnn hybrid method," *IEEE Transactions on Vehicular Technology*, vol. 70, no. 5, pp. 4252–4261, 2021.

[31] J. Qiao, X. Liu, and Z. Chen, "Prediction of the remaining useful life of lithium-ion batteries based on empirical mode decomposition and deep neural networks," *IEEE Access*, vol. 8, pp. 42 760–42 767, 2020.

[32] V. Sze, Y.-H. Chen, T.-J. Yang, and J. S. Emer, "Efficient processing of deep neural networks: A tutorial and survey," *Proceedings of the IEEE*, vol. 105, no. 12, pp. 2295–2329, 2017.

[33] S. Atalay, M. Sheikh, A. Mariani, Y. Merla, E. Bower, and W. D. Widanage, "Theory of battery ageing in a lithium-ion battery: Capacity fade, nonlinear ageing and lifetime prediction," *Journal of Power Sources*, vol. 478, p. 229026, 2020.

[34] Z. Shi, H. Liang, S. Huang, and V. Dinavahi, "Distributionally robust chance-constrained energy management for islanded microgrids," *IEEE Transactions on Smart Grid*, vol. 10, no. 2, pp. 2234–2244, 2018.

[35] A. Cuneo, V. Zaccaria, D. Tucker, and A. Traverso, "Probabilistic analysis of a fuel cell degradation model for solid oxide fuel cell and gas turbine hybrid systems," *Energy*, vol. 141, pp. 2277–2287, 2017.

[36] P. H. Hoang, G. Ozkan, P. R. Badr, L. Timilsina, B. Papari, and C. S. Edrington, "Integrating degradation forecasting into distribution grids' advanced distribution management systems," *International Journal of Electrical Power & Energy Systems*, vol. 150, p. 109071, 2023.

[37] The Economist, "Lithium battery costs have fallen by 98% in three decades," vol. 134, 2021. [Online]. Available: http://https://www.economist.com/

[38] E. Buraimoh, G. Ozkan, L. Timilsina, P. K. Chamarthi, B. Papari, and C. S. Edrington, "Overview of interface algorithms, interface signals, communication and delay in real-time co-simulation of distributed power systems," *IEEE Access*, 2023.